pp. 1–21 (2022)

# Computational mimicking of surgical leaflet suturing for virtual aortic valve neocuspidization

A. A. Liogky*†‡

**Abstract** — The aortic valve neocuspidization (AVNeo) procedure requires the design of patient-specific neocusps which can be made numerically through the neovalve closure modelling. Prior the simulation, it is required to 'suture virtually' the neocusps into the patient's aortic geometry, i.e., to find such state in which the neocusps are placed in the aortic root lumen without intersections of physical surfaces and neo-valve prolapse, and the position of the suture boundary satisfies the boundary conditions. To solve this problem, we tried to mimic neocusps suturing in Ozaki's operation. As a result, we propose a new algorithm for 'virtual suturing' of given neocusps, considered as thin shells. The approach is able to work with both small and large (compared to an optimal size) neocusps and to handle each cusp independently of the others.

**Keywords:** Aortic valve, leaflet suturing, mathematical modelling, virtual neocuspidization

**MSC 2010:** 92C10, 74K25

In recent years, aortic valve neocuspidization (AVNeo) procedure proposed by Ozaki et al. [19] has become popular. The approach is based on using leaflets from treated autologous pericardium to replace the aortic valve and have very low risk of tissue rejection in patients. Moreover, as shown in [3, 8, 25, 27], the procedure has a lot of other advantages, such as avoiding anticoagulation therapy, a low gradient of transvalvular pressure, an increased effective orifice area, minor regurgitation, normal dimensions of the aortic annulus and aortic root during cardiac cycle, low degradation and calcification, reproducibility, and a low cost.

Choosing an optimal leaflet size and form is the main problem of using AVNeo. If the leaflets are too small, then there is a risk of regurgitation in the neo-valve; if they are too large, then the neo-leaflets may cover the coronary orifices [17]. An optimal reconstructed neo-valve should provide normal aortic valve function and therefore should satisfy certain properties, i.e., no billowing, no regurgitation and etc., for details refer to [11, 12, 15, 22, 24].

Ozaki et al. proposed their own methodology for selecting the neo-leaflet tem-

*Marchuk Institute of Numerical Mathematics of the RAS, Moscow 119333, Russia

†Sirius University of Science and Technology, Sochi 354340, Russia

‡World-Class Research Center 'Digital biodesign and personalized healthcare', I. M. Sechenov First Moscow State Medical University (Sechenov University), Moscow 119992, Russia
E-mail: al.liogky@yandex.ru

The work was supported by the Russian Science Foundation (project No. 21-71-30023).

plates based on measurements of aortic root made by their sizer [19], but there is no guarantee that the proposed approach provides optimally sized neocusp templates. Moreover, it has been shown in echocardiography research that 12.5% of patients undergoing the AVNeo procedure develop thrombosis, which can also be caused by an excess neocusp area [6], i.e., non-optimality of the selected cusp templates.

To assess the degree of optimality of the neo-valve, it is necessary to evaluate its characteristics in the closed state. Numerical modelling of the diastolic state of the neo-valve can be used for the patient-specific design of optimal cusps. The process of modelling can be divided into several stages: (i) extraction from the patient's CT images of the inner surface of the aortic root and determination of the future cusp-aorta suture line on the aortic surface, (ii) finding the initial configuration of the cusps inside the aortic root ('virtual suturing' of the neo-cusps), (iii) performing numerical simulation of the aortic valve closure and, finally, (iv) estimation of the parameters of interest for the closed valve configuration. These estimated parameters may be used in an optimization procedure. By 'virtual suturing' in step (ii) we mean finding such configuration of the neo-valve, in which the neocusps are placed in the lumen of the aortic root without neo-valve prolapse, do not intersect with each other or with the surface of the aorta, the position of the cusp suture boundary satisfies specified boundary conditions. Since optimization procedure requires calculation of a solution for a sufficiently wide range of cusp template parameters, a 'virtual suturing' method applicable for different neocusps, is demanded. In the present paper we propose such a method.

Significant success in the technique of 'virtual suturing' was achieved for the operation of transcatheter aortic valve implantation (TAVI) providing expansion of a stent from a compressed state to the size of the aorta [16, 23] or expansion of the aortic lumen to the size of a stent [31]. However, these methods are not suitable for AVNeo surgery, since stents are not used in it, and the aorta does not change its diameter [30].

Besides the works on TAVI modelling, a few articles address the process of 'virtual suturing' and most of them study the behavior of the aortic valve for idealized geometries, avoiding the issue of 'virtual suturing' of the cusps. The simplest variant of the 'virtual suturing' is the 'contact planes of symmetry' method, which is used in symmetric geometries[13, 14] and therefore is not applicable for patient-specific geometries. An extension of this method to the case of a real aorta in the form of the 'virtual contact planes' method was proposed in [5]. However, this approach does not work properly with sufficiently large neocusps when the virtual planes are not the real surfaces of contact of the cusps (see Fig. 1). Moreover, the method may not work if the central line of the aorta inside the aortic root is very different from a straight line.

In this paper we propose a new computational algorithm for 'virtual suturing'. To this end, we mimic the neocusp's suturing from the procedure of neocuspidization proposed by Ozaki, by highlighting the features of the sutured neocusps. Then we formulate these features as mathematical constraints. We consider the aortic neocusps as thin membranes or Kirchhoff–Love shells made of a specific hyperelastic

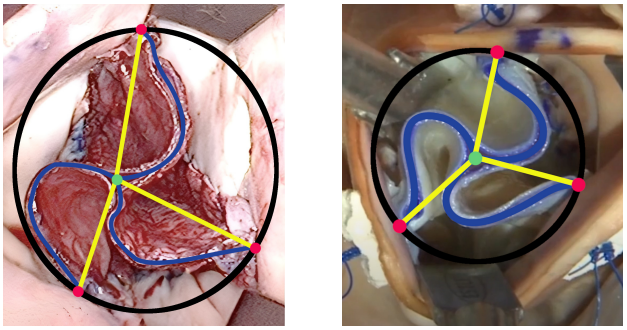

(a) (b)

**Figure 1.** Sutured configurations of the reconstructed aortic valve. The blue curves are leaflet contact lines that radiate from the triple contact point marked in green. Commissure points are marked in red. Possible positions of the virtual contact planes are marked in yellow and it can be seen that they are very different from the real contact surfaces. Black color marks the virtual circle passing through the commissure points. Photo (a) is taken from [20] and photo (b) is a screenshot from Ozaki's procedure training video [21].

material. As a result we have proposed a sequence of elastic problems for quasi-static equilibrium to be solved that consistently include more and more constraints and eventually lead to the desired state. The advantage of the proposed approach is its ability to work with both small and large (compared to optimal size) neocusps, which is achieved through the use of non-planar contact surfaces. Also, the method does not allow a strong sagging of the neocusp's free boundary below the plane of the commissures, which guarantees the absence of prolapse. In addition, the method imposes restrictions on the neocusps independently, and therefore the calculation of the position of each cusp can be performed in parallel.

The paper is organized as follows. In Section 1 we present the problem description and an algorithm for solving arising quasi-static equilibrium problems. In Section 2 we briefly overview the suturing of the neocusps in AVNeo procedure and discuss its features. In Section 3 we formulate the 'virtual suturing' algorithm. Results of numerical experiments are presented in Section 4. Limitations of the approach are given in Section 5.

## 1. Modelling of the cusp quasi-static equilibrium

### 1.1. Elastic nodal forces

A detailed description of elastic models is not the purpose of this article, we give a sketch of used modelling methods, for details we refer to [29].

We consider cusps as thin hyperelastic shells, which are described by the Kirchhoff–Love thin shell theory [26]. Within this theory, the right Cauchy–Green tensor $\mathbb{C}$ can be decomposed into in-plane $\mathbb{C}_S$ and out-of-plane $\mathbb{C}_N$ components [18, 26]:

$$\mathbb{C} = \mathbb{C}_S + \mathbb{C}_N. \tag{1.1}$$

Hyperelasticity implies that there is a potential $\psi(\mathbb{C})$ which determines an internal elastic energy of the material $U$. In the theory of thin incompressible shells it can be rewritten as a function $\widehat{\psi}(\mathbb{C}_S)$, and the variation of the internal elastic energy $\delta U$ due to displacements can be represented as

$$\delta U = \delta U_m + \delta U_b. \tag{1.2}$$

Here $\delta U_m$ is the membrane part of the energy variation describing an in-plane deformation of the cusp, and $\delta U_b$ is the bending part characterizing resistance of the shell to bending [29].

In this article, we aim to place three preset aortic valve cusp patterns inside the aortic volume avoiding their intersections. We do not aim to reproduce the actual position of the cusps inside the aorta under the influence of external forces. Although we are free to choose a material model, it should not be too rigid, to avoid problems with numerical instabilities. We have chosen St. Venant–Kirchhoff (SVK) material with zero Poisson's ratio $\nu = 0$, whose potential in the thin shell theory takes the form

$$\widehat{\psi}_{SVK}(I_1, J) = \frac{E}{8}\left((I_1 - 1)^2 - 2J^2 + 1\right) \tag{1.3}$$

where $I_1 = \operatorname{tr}\mathbb{C}_S$, $J^2 = \det\mathbb{C}_S$ and $E$ is Young's modulus.

The middle surface of the cusp is defined by its triangulation. Due to (1.2), at each node of a computational mesh with index $n$, the elastic force is a composition of the membrane $\boldsymbol{F}_n^m$ and bending $\boldsymbol{F}_n^b$ forces [29].

### 1.2. External nodal forces

The force of external pressure acting on the $n$th node of the cusp mesh is calculated using the following formula:

$$\boldsymbol{F}_n^p = \frac{P\sum_{i(n)} \boldsymbol{S}_i^t}{3} \tag{1.4}$$

where $P$ is applied diastolic pressure, $\sum_{i(n)} \boldsymbol{S}_i^t$ is the sum of all oriented areas of triangles sharing the $n$th node at the current configuration.

To confine the cusp inside a given constraint volume $\Omega$, we use additional forces that will restrict the cusp to remain in $\Omega$. Let $d_\Omega(\boldsymbol{x})$ be the signed distance field (SDF) to the boundary $\partial\Omega$ of the constraint volume

$$d_\Omega(\boldsymbol{x}) = \begin{cases} \min\limits_{\boldsymbol{y}\in\partial\Omega} ||\boldsymbol{x}-\boldsymbol{y}||, & \boldsymbol{x}\in\Omega \\ -\min\limits_{\boldsymbol{y}\in\partial\Omega} ||\boldsymbol{x}-\boldsymbol{y}||, & \text{otherwise} \end{cases}$$

and let $\boldsymbol{n}_\Omega(\boldsymbol{x}) = \nabla d_\Omega(\boldsymbol{x})$. Then the repulsion SDF-force acting on the $n$th node $\boldsymbol{Q}_n$ is

$$\boldsymbol{F}_n^{r,\Omega} = \frac{\eta_1 \sum_{i(n)} S_i^t}{3} f(d_\Omega(\boldsymbol{Q}_n))\, \boldsymbol{n}_\Omega(\boldsymbol{Q}_n), \qquad f(d) = \max\left(1 - \frac{2(d+\eta_3)}{\eta_2}, 0\right) \tag{1.5}$$

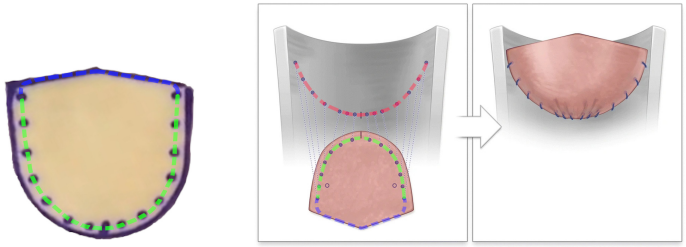

(a) (b)

**Figure 2.** Scheme of suturing in AVNeo. Green dotted line is cusp suture line (CSL), blue dotted line is free boundary of the cusp, pink dotted line is aortic suture line (ASL). Subfigure (a) shows flat template of the cusp and subfigure (b) shows the scheme of suturing the cusp in AVNeo procedure. Subfigure (a) is changed screenshot from [20] and (b) is modified picture from [2].

where $f(d)$ is a penalty function, coefficients $\eta_1$, $\eta_2$, and $\eta_3$ characterize the penalty force and the depth of immersion into the volume, and $\sum_{i(n)} S_i^t$ is the sum of areas of all triangles sharing the $n$th node at the current configuration.

To avoid valve prolapse, we introduce another artificial force that does not allow the free boundary of the cusp to sag too deeply. Let the cusp boundary consist of a free boundary and a suture boundary, and on the cusp in the initial planar state one chooses such an orthonormal cartesian coordinate system $\{\boldsymbol{e}_1, \boldsymbol{e}_2\}$ that $\boldsymbol{e}_1$ is parallel to $(\boldsymbol{N}_0 - \boldsymbol{N}_1)$, where $\boldsymbol{N}_0$ and $\boldsymbol{N}_1$ are the beginning and end of the suture boundary and $\boldsymbol{e}_2$ is oriented outwards of the suture boundary (see Fig. 4a). Let $\boldsymbol{P}_n = P_n^x \boldsymbol{e}_1 + P_n^y \boldsymbol{e}_2$ be an initial position of the $n$th node of the free boundary and $\boldsymbol{Q}_n$ is its current position. Let $\mathscr{M}$ be a plane of commissures with a unit normal $\boldsymbol{n}$ directed from the left ventricle towards the aorta, and $\boldsymbol{A}_0$ be one of the commissures, $\boldsymbol{A}_0 \in \mathscr{M}$. Then the free-boundary force acting on node $\boldsymbol{Q}_n$ is

$$\boldsymbol{F}_n^{f-b} = \eta_1 S^0 \frac{\sum_{i(n)} l^i_{\text{free}}}{2L_{\text{free}}} f((\boldsymbol{Q}_n - \boldsymbol{A}_0)\cdot\boldsymbol{n} - (\boldsymbol{P}_n - \boldsymbol{N}_0)\cdot\boldsymbol{e_2}) \tag{1.6a}$$

$$f(d) = \max\left(1 - \frac{2(d+\eta_3)}{\eta_2}, 0\right)\boldsymbol{n} \tag{1.6b}$$

where $S^0$ is the full area of the cusp and $L_{\text{free}}$ is the length of free boundary, $\sum_{i(n)} l^i_{\text{free}}$ is the sum of lengths of all free boundary edges sharing $\boldsymbol{Q}_n$ at the initial flat configuration, and $\eta_1$, $\eta_2$, $\eta_3$ characterize the penalty force and the depth of penetration through the plane $\mathscr{M}$.

### 1.3. Algebraic system with constraints

Let $\boldsymbol{Q} = (\boldsymbol{Q}_0^T, \boldsymbol{Q}_1^T, ..., \boldsymbol{Q}_{N-1}^T)^T$ be the coordinate vector of all nodes (degrees of freedom) of the cusp triangulation. Given all the forces applied to the mesh nodes, we can write down $N$ equilibrium equations for the cusp:

$$\boldsymbol{F}_n^m + c^b \boldsymbol{F}_n^b + \boldsymbol{F}_n^p + \boldsymbol{F}_n^{f-b} + \sum_{k=0}^{K-1} \boldsymbol{F}_n^{r,\Omega_k} = 0, \quad n = 0, \ldots, N-1 \tag{1.7}$$

where $c^b = 1$ and $c^b = 0$ for shell and membrane formulations, respectively, and $\Omega_k$, $k = 0, \dots, K-1$ are $K$ given constraint volumes. Equations (1.7) form a nonlinear algebraic system

$$\mathscr{F}(\boldsymbol{Q}) = 0. \tag{1.8}$$

We solve system (1.8) approximately using the inexact Newton method with the line search strategy from package Kinsol [7] supplemented by a linear solver MPT_ILUC from the framework INMOST [28]. Note that the approximate solution of the equilibrium problem is used to move the cusp to the constraint volume of the aortic root that we set and to weaken the local deformations of the cusps. Actually, we find a rough approximation $\boldsymbol{Q}^*$ to the solution of (1.8), which requires a few Newton iterations and provides a cusp with self-intersections. To avoid the latters, we apply the collision solver proposed by Bridson et al [4] for robust collision resolution and get a state $\boldsymbol{Q}^{**}$. The overall procedure is summarized in Algorithm 1.1.

**Algorithm 1.1** Approximate solution of quasi-static problem (1.8), SolveQSEProb

initial guess $\boldsymbol{G}$

1: Form nonlinear algebraic system $\mathscr{F}(\boldsymbol{Q}) = 0$
2: Solve approximately the system $\boldsymbol{Q}^* = \text{NonLinSolver}(\mathscr{F}, \boldsymbol{G})$
3: Resolve self-intersections $\boldsymbol{Q}^{**} = \text{ResolveSelfIntersections}(\boldsymbol{Q}^*, \boldsymbol{G})$
4: **return** $\boldsymbol{Q}^{**}$

## 2. Suturing in surgical AVNeo procedure

Prior suturing in the surgical AVNeo process, one prepares a cut from the treated pericardium template with marked points for making stitches (see Fig. 2). The line drawn through the marked points forms the cusp suturing line (CSL). The suturing process is represented by the following algorithm [1]:

1. Drop the cusp into the aorta (see Fig. 2b). Make the first suture passing through the center of CSL and the center of the corresponding future aortic suture line (ASL) on the aortic ring (see Fig. 3a).
2. Suture a half of the cusp:
   (a) Make sutures passing through the marked points on the template and the future ASL so that the ratio of the distance between the stitches on the template to the distance between the stitches on the aortic ring is 3:1. At the same time, push the template down underneath the remnant annulus (see Fig. 3b).
   (b) When the remainder of the CSL half length is equal to or slightly greater than the remainder of the future ASL half length, start making the sutures between the cusp and the aortic ring equidistant (see Fig. 3c).

(c) Make the last stitch passing through a point that is located at a distance of 5 mm from the free edge of the cusp and 2 mm below the highest point of the commissure on the ring.

(d) Adjust the position of the cusp towards the aortic wall.

3. Repeat Step 2 for the second half of the template.

4. Repeat Steps 1 and 2 for the half of the second cusp approaching the first cusp.

5. Creating a commissure between the first and second cusp. After this step, the end of the CSL will be brought to the end of the ASL (see Fig. 3d)

6. Repeat Step 2 for the second half of the second template.

7. Repeat Steps 1, 2, and 5 for the first half of the third template, and then Steps 2 and 5 for the second half of the third template.

8. Adjust the positions of each commissure to ensure the best configuration and coaptation of the tricuspid valve (see Fig. 1b) .

Important features of this procedures are:

- Nonlinear CSL-to-ASL mapping. The mapping of the points of CSL to ASL is non-linear in terms of the curve lengths, although the curve length distortion function resulting from the mapping is piecewise constant.

- Fixed near-CSL tangent half-plane. Lowering the template into the left ventricular cavity in Step 1 and pushing the template down in Step 2 results in lining of the sutured cusp part near the CSL on the aortic surface so as to provide more downward deflection towards the left ventricle. This should be taken into account when setting boundary conditions in shell models, as this may have a significant impact on the resulting coaptation (for example, an incorrectly chosen lining direction led to inappropriate coaptation results for the shell model [29]).

- Complex non-planar cusp-to-cusp contact surfaces (see Fig. 1).

## 3. Virtual suture algorithm

### 3.1. Input geometry

Let an initial planar template $S_c^i$ of the $i$th cusp, $i = 0, 1, 2$, be defined by two boundaries $\boldsymbol{r}^i_{\text{csl}}(t) : [0,1] \to \mathbb{R}^2$ and $\boldsymbol{r}^i_{\text{free}}(t) : [0,1] \to \mathbb{R}^2$ where the first boundary represents

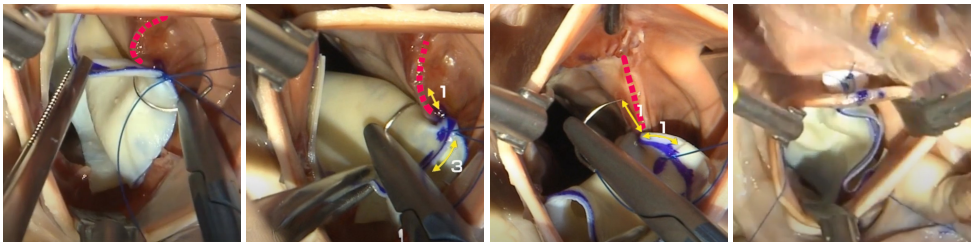


(a) (b) (c) (d)

**Figure 3.** Procedure of suturing in surgical AVNeo. The pink dotted line shows the future aortic suture line of the cusp. Subfigure (a) shows the process of making the first suture; subfigures (b) and (c) demonstrate the process of making sutures with a distance ratio between stitches on the cusp and the aortic ring 3:1 and 1:1, respectively; subfigure (d) shows the result of making a commissure between two cusps. All photos are modified screenshots from [21].

CSL and the second one is the free edge of the cusp (see Fig. 4a). These curves satisfy to $\boldsymbol{r}^i_{\text{csl}}(0) = \boldsymbol{r}^i_{\text{free}}(0)$, $\boldsymbol{r}^i_{\text{csl}}(1) = \boldsymbol{r}^i_{\text{free}}(1)$ and do not self-intersect or intersect each other at internal points. We denote by $H^i$ the $i$th cusp thickness.

Let a constraint volume $\Omega_a$ be a truncated part of the aorta including the aortic root, $\partial\Omega_a = S_r \cup S_i \cup S_o$, where $S_r$ is the internal surface of the aortic root, $S_i$ and $S_o$ are the inlet and outlet cross-sections of $\Omega_a$ (see Fig. 4b).

Functions $\boldsymbol{r}^i_{\text{asl}}(t) : [0,1] \to \mathbb{R}^3 \cap S_r$, $i = 0,1,2$, representing ASL of the $i$th cusp, parameterize continuous curves without self-intersections, the distance between curves $\boldsymbol{r}^i_{\text{asl}}$ and $\boldsymbol{r}^j_{\text{asl}}$, $i \neq j$, is not less than $H^{ij} = (H^i + H^j)/2$. The parameterization of curves $\boldsymbol{r}^i_{\text{asl}}$ is chosen so that when looking at the aortic lumen towards the left ventricle, the point on the curve moves counterclockwise with an increase of the parameter and the indexing of the curves is such that both points $\boldsymbol{r}^i_{\text{asl}}(1)$ and $\boldsymbol{r}^{(i+1)\%3}_{\text{asl}}(0)$ form a common commissure (where '%' means the remainder of the division).

To specify the clamped boundary condition, we introduce the tangent direction of $\boldsymbol{r}^i_{\text{asl}}$ curve $\tau^i_{\text{asl}}(t) = (\mathrm{d}\boldsymbol{r}^i_{\text{asl}}/\mathrm{d}t)\big/||\mathrm{d}\boldsymbol{r}^i_{\text{asl}}/\mathrm{d}t||$ , the unit normal $\boldsymbol{n}_{S_r}$ to the surface $S_r$ directed inside the region $\Omega_a$. Then we define the field $\boldsymbol{b}^i_{\text{asl}}(t) : [0,1] \to \mathbb{S}^2$, which is required to specify the clamped boundary condition, as $\boldsymbol{b}^i_{\text{asl}}(t) = \tau^i_{\text{asl}}(t) \times \boldsymbol{n}_{S_r}(\boldsymbol{r}^i_{\text{asl}}(t))$. The clamped boundary condition at a point of the sutured boundary $\boldsymbol{r}^i_{\text{asl}}(t)$ defines the tangent half-plane to the cusp passing through this point as follows:

$$\boldsymbol{r}_t(u,v) = u\boldsymbol{\tau}^i_{\text{asl}}(t) - v\boldsymbol{b}^i_{\text{asl}}(t),\ u \in \mathbb{R},\ v \in \mathbb{R}_+. \tag{3.1}$$

The introduced objects are defined via their discrete counterparts: $S^{i,h}_c$ is a planar triangulation of the $i$th cusp, $\boldsymbol{r}^{i,h}_{\text{csl}}(t)$ and $\boldsymbol{r}^{i,h}_{\text{free}}(t)$ are piecewise linear curves, $S^h_r$ is a triangulation of the aortic root surface, $\boldsymbol{r}^{i,h}_{\text{asl}}(t)$ is a piecewise linear curve with nodes on $S^h_r$, $\boldsymbol{b}^{i,h}_{\text{asl}}$ is a piecewise constant function. Hereinafter we omit superscript $h$ indicating discrete objects.

We also introduce auxiliary objects (see Fig. 4b):

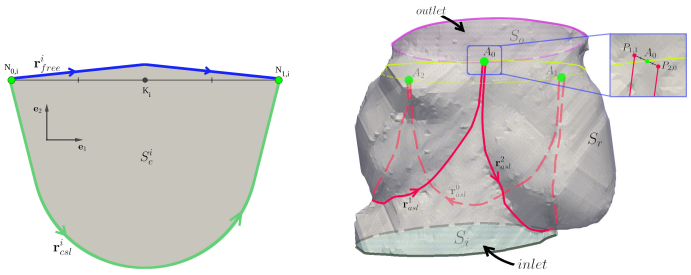


(a) (b)

**Figure 4.** Input geometry. Subfigure (a) shows the schematic geometry of the $i$th initial planar cusp template where the green line is CSL and the blue line is the free boundary. Subfigure (b) depicts a constraint volume of the aortic root. The dashed parts of the lines indicate invisible parts of the lines. The dark green and violet lines shows the boundaries of the inlet and outlet parts, respectively. The red lines are ASLs; the yellow line is a cut of the aortic root by the plane of commissures. The zoomed section shows the position of the commissure point $A_0$ with respect to the ends of the cusp suturing lines.

- $P_{0,i} = \boldsymbol{r}^i_{\text{asl}}(0)$, $P_{1,i} = \boldsymbol{r}^i_{\text{asl}}(1)$ are the local points of commissure of the $i$th cusp;
- $N_{0,i} = \boldsymbol{r}^i_{\text{csl}}(0)$, $N_{1,i} = \boldsymbol{r}^i_{\text{csl}}(1)$ are the $i$th cusp corners;
- $A_i = (P_{1,(i+1)\%3} + P_{0,(i+2)\%3})/2$ is the midpoint of the commissure;
- $\boldsymbol{M} = \text{aff}(A_0, A_1, A_2)$ is the plane of commissures with the normal $\boldsymbol{n} = \frac{(A_1 - A_0)\times(A_2 - A_0)}{||(A_1 - A_0)\times(A_2 - A_0)||}$;
- $R$ is the radius of the circumscribed circle for triangle $A_0A_1A_2$;
- $\text{len}_{\boldsymbol{r}}(t) = L(\boldsymbol{r}, t) = \int_0^t ||\,\mathrm{d}\boldsymbol{r}(t')/\,\mathrm{d}t'||\,\mathrm{d}t'$ is the length function of curve $\boldsymbol{r}$;
- $(\varphi_{\text{natural}} \circ \boldsymbol{r})(s) = \boldsymbol{r}(\text{len}^{-1}_{\boldsymbol{r}}(s))$ is the natural parameterization of curve $\boldsymbol{r}$;
- $(\varphi_{scl}(a) \circ \boldsymbol{r})(s) = \boldsymbol{r}(s \cdot a)$ is the $a$-scaling parameterization of curve $\boldsymbol{r}$.

Whenever possible, for the sake of brevity we shall omit the cusp index and write $S_c$, $\boldsymbol{r}_{\text{csl}}$, $\boldsymbol{r}_{\text{free}}$, $H$, $\boldsymbol{b}_{\text{asl}}$, $N_0$, $N_1$, $P_0$, $P_1$.

### 3.2. Suturing a cusp

At this step, we impose boundary conditions on the cusp template and expand it deep into the aorta.

Given the midpoint $K$ of segment $N_0N_1$, the midpoint $L$ of segment $A_1A_2$ and an initial planar cusp mesh $S_c^{(1,0)}$, we perform the following steps (see Fig. 5):

1. Shift and rotate $S_c^{(1,0)}$ to get a planar mesh $S_c^{(1,1)}$ with the following properties (see Fig. 5a):

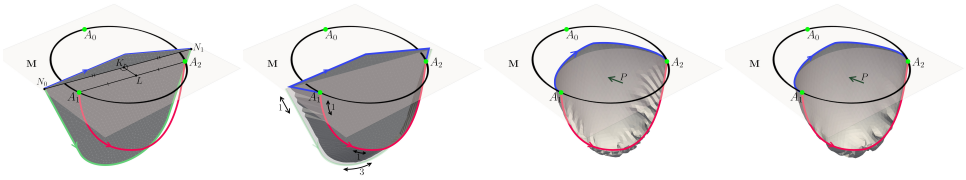

(a) (b) (c) (d)

**Figure 5.** Step 1 of the virtual suturing of the 0th cusp. The black circle passing through the green points of the commissures, lies in the plane $\boldsymbol{M}$. The red line is ASL, the green line is CSL, the blue line is the free boundary of the cusp. Subfigure (a) shows the initial planar cusp position after shifts and rotations. Subfigure (b) depicts the setting of the new position of the cusp sutured line. Double-sided arrows show cusp-to-aorta suture line distance relations. Subfigures (c) and (d) demonstrate results of solving quasi-static elastic problem in the membrane and shell formulations, respectively.

- Segment $N_0N_1$ lies in the plane $\boldsymbol{M}$ parallel to $A_1A_2$, and $\|N_0A_1\| < \|N_1A_1\|$.
- Vector $\overrightarrow{LK}$ is orthogonal to $N_0N_1$ and $(\overrightarrow{LK}, \overrightarrow{A_1A_0}) > 0$.
- The plane of $S_c^{(1,1)}$ is orthogonal to $\boldsymbol{M}$ and is oriented so that CSL and ASL are in the same half-space of the plane $\boldsymbol{M}$.
- $\|\overrightarrow{LK}\| = (c^0 + c^1 k)R$, where $k$ is a minimal non-negative integer such that $S_c^{(1,1)}$ does not intersect curve $\boldsymbol{r}_{\text{asl}}(t)$, $c^0 = 1.0$ and $c^1 = 0.1$ are predefined constants.

2. Suture CSL to ASL.
Surgical suturing in AVNeo procedure defines cusp-to-annulus stitching ratio $\alpha_{sl} = 3.0$ near the middle of the suture line and $\alpha_{sl} = 1.0$ near the ends of the suture line. We assume that for lengths $l_a$ of ASL and $l_c$ of CSL it holds $\alpha_{sl}^{-1} < J_{sl} = l_a/l_c < 1$, otherwise the selected template is too small or too large. For $\bar{\boldsymbol{r}}_{\text{asl}}(s) = (\varphi_{\text{natural}} \circ \boldsymbol{r}_{\text{asl}})(s)$ and $\bar{\boldsymbol{r}}_{\text{csl}}(s) = (\varphi_{\text{natural}} \circ \boldsymbol{r}_{\text{csl}})(s)$ the cusp-to-annulus mapping may be expressed as

$$\varphi : \bar{\boldsymbol{r}}_{\text{csl}}(s) \to \bar{\boldsymbol{r}}_{\text{asl}}(\gamma(s))$$

with a positive monotone function $\gamma : [0, l_c] \to [0, l_a]$. Then the curve length distortion function is

$$\chi(s) = \frac{||\,\mathrm{d}\bar{\boldsymbol{r}}_{\text{asl}}(\gamma(s))||}{||\,\mathrm{d}\bar{\boldsymbol{r}}_{\text{csl}}(s)||} = \frac{||\,\frac{\mathrm{d}\bar{\boldsymbol{r}}_{\text{asl}}}{\mathrm{d}\gamma}\frac{\mathrm{d}\gamma}{\mathrm{d}s}||}{||\,\frac{\mathrm{d}\bar{\boldsymbol{r}}_{\text{csl}}}{\mathrm{d}s}||} = \frac{\mathrm{d}\gamma}{\mathrm{d}s}.$$

We introduce the normalized length distribution function $\rho(\vartheta) : [0,1] \to \mathbb{R}_+$ such that

$$\rho(\vartheta) = \frac{l_c}{l_a}\chi(\vartheta l_c) = J_{sl}^{-1} \cdot \chi(\vartheta l_c)$$

$$\int_0^1 \rho(\vartheta)\,\mathrm{d}\vartheta = \int_0^1 \frac{l_c}{l_a}\chi(\vartheta l_c)\,\mathrm{d}\vartheta = \frac{1}{l_a}\int_0^{l_c} \chi(s)\,\mathrm{d}s = \frac{\gamma(l_c) - \gamma(0)}{l_a} = \frac{l_a - 0}{l_a} = 1.$$

The cusp-to-annulus stitching ratios ($\chi(0) = \chi(1) = 1.0,\ \chi(\frac{1}{2}l_c) = \alpha_{sl}^{-1}$) and the normalization conditions

$$\rho(0) = \rho(1) = J_{sl}^{-1}, \qquad \rho(0.5) = \alpha_{sl}^{-1} J_{sl}^{-1}, \qquad \int_0^1 \rho(\vartheta)\,\mathrm{d}\vartheta = 1$$

provide the following function

$$\rho(\vartheta) = \begin{cases} J_{sl}^{-1}, & |\vartheta - 0.5| \geqslant \dfrac{\alpha_{sl}(1 - J_{sl})}{2(\alpha_{sl} - 1)} \\ \alpha_{sl}^{-1} J_{sl}^{-1}, & \text{otherwise.} \end{cases}$$

Finally, for each $S_c^{(1,1)}$-mesh node $n$ lying on the CSL-boundary, we calculate its parameter $s_{\mathrm{csl}}^n$ with respect to the piecewise linear $\bar{\boldsymbol{r}}_{\mathrm{csl}}$ curve and set a new position $\boldsymbol{r}^n = \bar{\boldsymbol{r}}_{\mathrm{asl}}(\gamma^n)$ of the node, where $\gamma^n = l_a \int_0^{s_{\mathrm{csl}}^n / l_c} \rho(\vartheta)\,\mathrm{d}\vartheta$. The resulting mesh is denoted by $S_c^{(1,2)}$.

3. Solve the static equilibrium problem in the membrane formulation.
Impose Dirichlet boundary condition on the sutured boundary of the cusp and the free boundary condition on the other part of boundary, apply the diastolic pressure force (1.4) and the free-edge-penalty force (1.6) to avoid the fall of the cusp inside the aorta. Solve approximately the problem of quasi-static equilibrium of the cusp in the membrane formulation; to this end, apply the hyperelastic nodal force method with the St. Venant–Kirchhoff potential (1.3). The resulting nonlinear system is solved with the initial guess $S_c^{(1,2)}$ and the initial unloaded configuration of the cusp $S_c^{(1,0)}$. The resulting mesh is denoted by $S_c^{(1,3)}$. Since the cusp may undergo large displacements, the collision solver may fail. In this case one solves a sequence of similar problems, where Dirichlet condition on CSL-boundary is sequentially shifted from position on $S_c^{(1,1)}$ to position on $S_c^{(1,2)}$.

4. Solve the static equilibrium problem in the shell formulation.
The clamped boundary condition on the sutured boundary uses vector field $\boldsymbol{b}_{\mathrm{asl}}$ interpolated from ASL to CSL at Step 2. To take into account the clamped boundary condition, solve approximately the quasi-static equilibrium problem of the thin Kirchhoff–Love shell using the same hyperelastic potential (1.3) and get the surface mesh $S_c^{(1,4)}$. The final mesh is denoted by $S_c^{(1)}$.

### 3.3. Contact constraints

In order to guarantee that three deformed cusps do not intersect each other, we define three nonintersecting constraint volumes. Repulsion force (1.5) makes each cusp to belong to its constraint volume and thus provides their non-intersection.

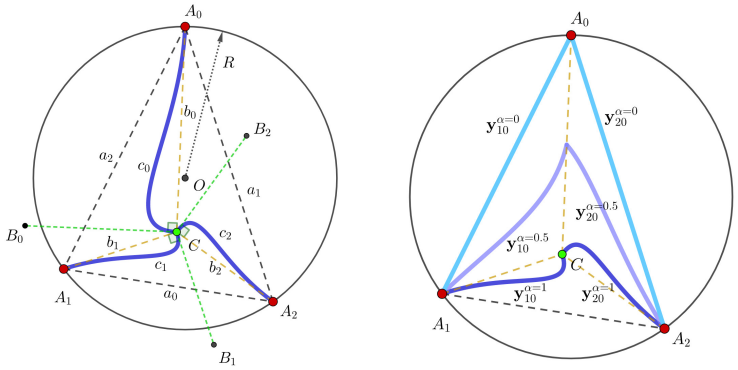


**Figure 6.** Subfigure (a) shows the intersection of a tightly closed tricuspid aortic valve with the plane of commissures and auxiliary geometric constructions. The blue lines depict slices of the cusp surfaces and $C$ is the point of cusp triple contact. The black circle centered at point $O$ passes through the red points of the commissure. Subfigure (b) shows position of parametric curves $\mathbf{y}_{10}^{\alpha}$ and $\mathbf{y}_{20}^{\alpha}$ for $\alpha = 0,\ 0.5,\ 1.0$.

The constraint volume is defined by contact surfaces which are formed by their intersections with the plane of commissures $\boldsymbol{M}$. The latter three curves are defined by the position of point $C$ of the triple contact of the cusps on the plane $\boldsymbol{M}$ (see Fig. 6a). If point $C$ of the triple contact does not exist, the valve is incompetent and its assessment makes no sense. Figure 6a shows basic geometric objects on the commissural plane $\boldsymbol{M}$: the intersection of $\boldsymbol{M}$ and the contact surface of the $i$th and $j$th cusp is a curve $\widehat{A_kC}$ of length $c_k$, the length of the intersection of $\boldsymbol{M}$ and the $i$th cusp is $l_i$, the length of segment $A_jA_k$ is $a_i$. Hereinafter $(i,j,k)$ is a positive permutation of numbers $(0,1,2)$. The following geometric relations hold:

$$\begin{cases} l_0 = c_1 + c_2 \\ l_1 = c_2 + c_0 \\ l_2 = c_0 + c_1 \end{cases} \quad \Leftrightarrow c_k = (l_i + l_j)/2 - l_k.$$

It is clear that $l_i$ should be geometrically consistent, otherwise $c_k$ may be negative.

The ideal position of the contact surfaces of the cusps (which surgeons are trying to achieve in surgical AVNeo Step 8, see Section 2) makes each cusp aligned along the corresponding intersection curve. Finally, since the cusp is deformed so that it does not experience large billowing towards the left ventricle, we can assume that the intersection curve mapped onto the undeformed planar configuration of the cusp, is close to the segment $N_{0,i}N_{1,i}$ and therefore its length is known: $l_i = ||N_{0,i}N_{1,i}||$.

**3.3.1. The common point of virtual contact surfaces on the plane of commissures.** For length $b_i$ of segments $A_iC$ the relations $b_i \leqslant c_i$ hold and point $C$ belongs to triangle $\triangle A_0A_1A_2$, otherwise the valve is incompetent. These two conditions give

restrictions on admissible positions of point $C$. The next proposition defines point $C$ explicitly.

**Proposition 3.1.** *Let point $K_i$ divide the segment $A_jA_k$ in the ratio $c_j$ to $c_k$ and $v_i = ||A_jA_k||/(c_j + c_k)$. Then*

1. *if for some $i$ we have $||A_iK_i|| < v_ic_i$, then $C = K_i$ and $||A_jC|| \leqslant v^*c_j$, $j = 0,1,2$, with $v^* = v_i$;*
2. *if for some $i = 0,1,2$ we have $||A_iK_i|| \geqslant v_ic_i$, then there exists a unique $C \in \triangle K_0K_1K_2 \subset \triangle A_0A_1A_2$ satisfying the triple equality*

$$\frac{||A_0C||}{c_0} = \frac{||A_1C||}{c_1} = \frac{||A_2C||}{c_2} \tag{3.2}$$

*and $||A_jC|| \leqslant v^*c_j$, $j = 0,1,2$, with $v^* = ||A_iC||/c_i$, $i = 0,1,2$.*

**Remark 3.1.** If $\triangle A_0A_1A_2$ is not an obtuse triangle and $c_0 = c_1 = c_2$, then $C$ is the center of the circumscribed circle.

Although Proposition 3.1 assures existence of $C$ such that $b_i \leqslant v^*c_i$, for $v^* > 1$ such point corresponds to an incompetent valve with possible regurgitation due to small sizes of the cusps. The next proposition gives sufficient conditions for competent valves.

**Proposition 3.2.** *Let $l_i = \alpha a_i$ with certain factor $\alpha > 0$ be chosen for $i = 0,1,2$. Then*

1. *the triple contact point $C$ satisfies* (3.2) *and its position does not depend on $\alpha$;*
2. *if $\alpha \geqslant 2/\sqrt{3}$, then $v^* \leqslant 1$, i.e., $b_i \leqslant c_i$, $i = 0,1,2$.*

**Remark 3.2.** Under assumptions of Proposition 3.2, point $C$ is the 1st dilation center of the $\triangle A_0A_1A_2$ [10, X(3513)].

Proposition 3.2 suggests to choose the cusps such that $l_i = \alpha a_i$ with $\alpha > 1.16$ which provides existence of the triple contact point $C$.

**3.3.2. Virtual contact surfaces.** Virtual contact surfaces are repulsion surfaces in the 'virtual suturing' algorithm which allows us to place the cusps independently within the aortic lumen while ensuring that there is no overlap between the cusp surfaces. Intersection of the contact surfaces with the plane of commissures is given by $\widehat{A_iC}$ curves (see Fig. 6). According to clinical evidence, these curves have a consistent deflection clockwise or counterclockwise. For definiteness, we further

assume that the deflection is counterclockwise, i.e., the curve $\widehat{A_iC}$ is located inside the corner segment $A_iCA_j$ with $j=(i+1)\%3$. Let $B_i$ be a point located at distance $d_i=\min(R,||CA_j||)$ from $C$ and lying on the ray $CA_j$ if the angle $\angle A_iCA_j \leqslant \pi/2$ and on the ray lying inside the corner segment and orthogonal to the segment $CA_i$ otherwise (see Fig. 6a). We consider a Bezier curve $\boldsymbol{y}_i=\boldsymbol{y}_i^{\sigma^*}(t)$, $t\in[0,1]$:

$$Y_i^0=C,\quad Y_i^1=C+\sigma(B_i-C),\quad Y_i^2=C+\frac{\sigma}{\omega+\sigma}(A_i-C),\quad Y_i^3=A_i \tag{3.3a}$$

$$\boldsymbol{y}_i^\sigma(t)=\sum_{k=0}^{3}Y_i^k b_k^3(t),\quad b_k^n=\frac{n!}{(n-k)!k!}t^k(1-t)^{n-k} \tag{3.3b}$$

where $\omega$ is an adjustable positive parameter ($\omega=0.5$ hereinafter), and

$$\sigma^*=\min(\arg\min_{\sigma\geqslant 0}|L(\boldsymbol{y}_i^\sigma,1)-l_i|). \tag{3.3c}$$

The Bezier curve is linearly extended for $t>1$:

$$\widetilde{\boldsymbol{y}}_i(t)=\begin{cases}\boldsymbol{y}_i^\sigma(t), & t\in[0,1]\\ A_i+(A_i-C)(t-1), & t>1.\end{cases}$$

If the shape of the aorta root is close enough to cylindrical, the surface defined by two parameters $t,u$:

$$\boldsymbol{G}_i(t,u)=\widetilde{\boldsymbol{y}}_i(t)-u\boldsymbol{n},\quad t\geqslant 0,\quad u\in\mathbb{R} \tag{3.4}$$

does not intersect the suturing lines $r^j_{\text{asl}}$ and $r^k_{\text{asl}}$. In this case $\boldsymbol{G}_i$ is a proper contact surface. Otherwise, the definition of the surface should be modified; the general approach for defining $\boldsymbol{G}_i$ will be presented elsewhere.

The surface constructed by formula (3.4) may deviated considerably from a plane and the numerical solution of the quasi-static equilibrium problem with the repulsion forces may fail. To cope with this, we approach to the constructed surface $\boldsymbol{G}_i(t,u)$ sequentially, starting from a planar surface. Let us consider the following family $\boldsymbol{y}_{ij}^\lambda$ of curves, $i,j=0,1,2$ (see Fig. 6b):

$$\boldsymbol{y}_{ij}^\lambda=\sum_{k=0}^{3}Y_{ij}^k(\lambda)b_k^3,\quad Y_{ij}^k(\lambda)=\lambda Y_i^k+(1-\lambda)Z_{ij}^k \tag{3.5a}$$

$$\widetilde{\boldsymbol{y}}_{ij}^\lambda=\begin{cases}\boldsymbol{y}_{ij}^\lambda, & t\in[0,1]\\ A_i+(A_i-Y_{ij}^2(\lambda))(t-1), & t>1\end{cases},\quad \begin{gathered}Z_{ij}^0=A_j,\quad Z_{ij}^1=\tfrac{2}{3}A_j+\tfrac{1}{3}A_i,\\ Z_{ij}^2=\tfrac{1}{3}A_j+\tfrac{2}{3}A_i,\quad Z_{ij}^3=A_i.\end{gathered} \tag{3.5b}$$

The family of curves $\widetilde{\boldsymbol{y}}_{ij}^\lambda$ generates the family of surfaces

$$\boldsymbol{G}_{ij}^\lambda(t,u)=\boldsymbol{y}_{ij}^\lambda(t)-u\boldsymbol{n},\quad t\geqslant 0,\quad u\in\mathbb{R}. \tag{3.6}$$

The surface $\boldsymbol{G}_{ij}^0$ is a half-plane, the surface $\boldsymbol{G}_{ij}^1$ is a contact surface. Iterative increasing of parameter $\lambda$ from 0 to 1 with subsequent solution of the quasi-static equilibrium problem accounting the repulsion surface $\boldsymbol{G}_{ij}^\lambda$, provide small displacements of the cusps between successive iterations and the overall robustness of the suturing algorithm. The sign distance to a contact surface $\boldsymbol{G}_i^\lambda(t,u)$ can be calculated efficiently, since finding real roots of the 5th degree polynomial is provided by the Jenkins–Traub algorithm [9].

### 3.4. Contact and volume constraints algorithm

Let thresholds $0 < v_{\min} < 1$ and $v_{\max} > 1$ be given. We summarize the virtual suturing algorithm as follows.

1. Find point $C$ and parameter $v^*$ in $\triangle A_0A_1A_2$ satisfying Proposition 3.1.
   If the solution does not satisfy (3.2) then the given cusps are unable to form a normally functioning tricuspid valve. If $v^* > v_{\max}$, then the valve can not close tightly that results in regurgitation. If $v^* < v_{\min}$, then the cusps are too large for the aorta. In both cases the provided configurations of the cusps should be discarded.

2. Apply the contact surface constraint.
   Denote the current guess to the cusp surface mesh by $S_c^{(2,1,0)} = S_c^{(1)}$. Sequentially increase parameter $\lambda_m$ from $\lambda_1 = 0$ to $\lambda_M = 1$ and for each $\lambda_m$ solve the problem of quasi-static equilibrium of the cusp with repulsive forces (1.5) from the surfaces $\boldsymbol{G}_{10}^\lambda$ and $\boldsymbol{G}_{20}^\lambda$ using $S_c^{(2,1,m-1)}$ as the initial guess denote the result as $S_c^{(2,1,m)}$. Set $S_c^{(2,1)} = S_c^{(2,1,M)}$.

3. Apply the aortic root constraints.
   Compute the sign distance function for the surface of the control volume $\Omega_a$. Until the cusp surface is entirely within the control volume $\Omega_a$, iteratively increase parameter $\eta_1$ in (1.5) and solve the quasi-static equilibrium problem of equilibrium with repulsive forces from the surfaces $\boldsymbol{G}_1, \boldsymbol{G}_2$, and SDF-forces to push the cusps into the domain $\Omega_a$, using the result of the previous iteration as the initial guess. Denote the resulting mesh of the cusp after the iterations as $S_c^{(2)} := S_c^{(2,2)}$.

The first step of the suturing algorithm 'sutures' the cusp to a given line without imposing restrictions on the cusp displacement from other cusps or the aorta. Then an allowable region is constructed for each cusp. The algorithm places the cusp in this region at the second step and in the aortic root region at the third step.

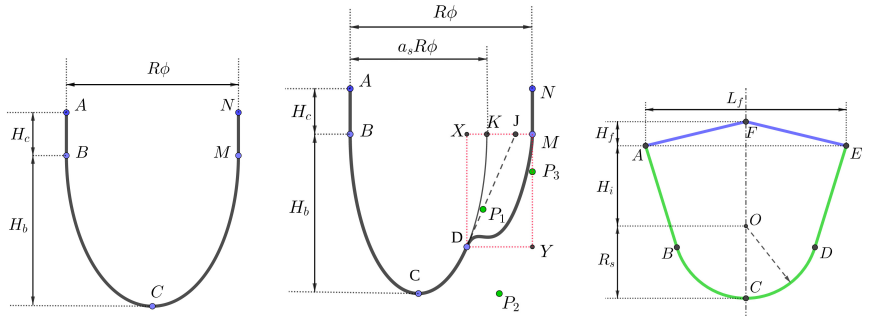


(a) (b) (c)

**Figure 7.** Subfigure (a) shows geometry of type A aortic suture line unfolding, $AB$ and $MN$ are straight segments, and $\widehat{BCM}$ arc is a half of an ellipse; Subfigure (b) shows geometry of type B aortic suture line unfolding. The line includes straight segments $AB$ and $MN$, $\widehat{BCD}$ arc (a part of a half of an ellipse $\widehat{BCK}$), and 4th order Bezier curve $\widehat{DM}$ determined by points $D,\ P_1,\ P_2,\ P_3,\ M$; Subfigure (c) describes the geometry of cusp templates with parameters $L_f, H_f, H_i, R_s$. $\widehat{ABCDE}$ is cusp sutured line and $\widehat{AFE}$ is the free boundary of the cusp.

## 4. Numerical experiments

### 4.1. Initial geometry

The present section presents three numerical experiments, which demonstrate performance of the proposed algorithm. In all cases, the aortic root is considered to be an ideal cylinder with radius $R = 12$ mm. The commissure points $A_0, A_1, A_2$ are chosen on the cross-section of the cylinder so that the sides of the triangle $A_0A_1A_2$ are related in a chosen proportion $a_0 : a_1 : a_2$. The thickness of the cusps is assumed to be $H = 0.5$ mm, and the distance between adjacent ends of the aortic suture lines (ASL) is also equal to $H$.

ASLs are defined by their unfolding from a cylindrical surface to a plane, and two types of lines are considered, type A line (see Fig. 7a) and type B line (see Fig. 7b). In the experiments the ASL parameters $H_c = 2.5$ mm and $H_b = 10$ mm are fixed, $R = 12$ mm is the radius of the aortic root, $a_s = 0.8$ for the type B curve and $\varphi$ is determined by the ratio of the sides of the commissural triangle and the distance between the ends of adjacent ends of the ASLs for every sutured line (see Figs. 7a and 7b).

The geometry of the cusps is given by a 4-parameter template (see Fig. 7c), with parameters $H_f = 2.5$ mm and $H_i = 11.5$ mm. The triangular mesh for each cusp has mesh size $h = 0.7$ mm.

All experiments exploit the same parameters for the nodal forces and the solvers (see Table 1). Parameter $\lambda_m = 0.1m$, $m = 0, \ldots, 10$.

**Table 1.** Nodal forces parameters and solver's parameters.

| | | | |
|---|---|---|---|
| Elastic force | $E$ | | |
| | 1000 kPa | | |
| pressure force | $P$ | | |
| | 8 kPa | | |
| free-edge force | $\eta_1$ | $\eta_2$ | $\eta_3$ |
| | 80 kPa | 0.1 mm | 0 mm |
| aortic domain sdf-force | $\eta_1$ | $\eta_2$ | $\eta_3$ |
| | 8 kPa | 0.5 mm | 0.5 mm |
| contact surface sdf-force | $\eta_1$ | $\eta_2$ | $\eta_3$ |
| | 16 kPa | 0.1 mm | 0 mm |

| Nonlinear solver (KinSol) | | Linear solver (INMOST) | |
|---|---|---|---|
| SolveStrategy | LineSearch | SolverType | mpt_iluc |
| NumMaxIters | 50 | drop_tol | 8e−3 |
| ScaledStepTol | 1e−5 | reuse_tol | 8e−4 |
| FuncNormTol | 1e−5 | | |
| MaxSetupCalls | 1 | | |

### 4.2. Experiment 1: suturing large symmetric cusps

In this experiment, we use three identical cusp templates with $L_f = 39$ mm and $R_s = 16.5$ mm (see Fig. 7c), sutured along ASL of type A, so that $a_0 = a_1 = a_2$.

For such configuration, the virtual contact planes method fails: the Newton method diverges. At the same time, the proposed suturing algorithm 'sutures' the cusps successfully (see Fig. 8a). Moreover, the resulting configuration is already close to the diastolic configuration of the valve.

### 4.3. Experiment 2: suture of different cusps

We consider three different cusp templates suturing to ASL of type B of different sizes, with the sizes of the cusps being specifically inconsistent with the sizes of the ASLs. Namely, we choose $a_0 : a_1 : a_2 = 8 : 9 : 6$ and $L_f^i = \gamma^i l_f$, $R_s^i = \gamma^i r_s$, $r_s = 33$ mm, $l_f = 39$ mm, where $\gamma^0 : \gamma^1 : \gamma^2 = 6 : 4 : 5$ and $\gamma^1 = 1$. The proposed algorithm coped with the placement of the cusps inside the aortic region without intersections (see Fig. 8b), however, the resulting state is not very close to the diastolic configuration. Nevertheless, the resulting state satisfies the requirements for the suturing algorithm and therefore can be used for further work.

### 4.4. Experiment 3: 'quasi-optimal' cusps

Proposition 3.2 sets the 'quasi-optimal' intercommissural cusp length as $L_f^i = 2a_i/\sqrt{3}$. We performed calculations with cusps of this length, taking the ratio $L_f^i : R_s^i = 13 : 11$ fixed and choosing $a_0 : a_1 : a_2 = 6 : 4 : 5$ for ASL curves of type A. The resulting contact surface in this case is very close to the plane and at the

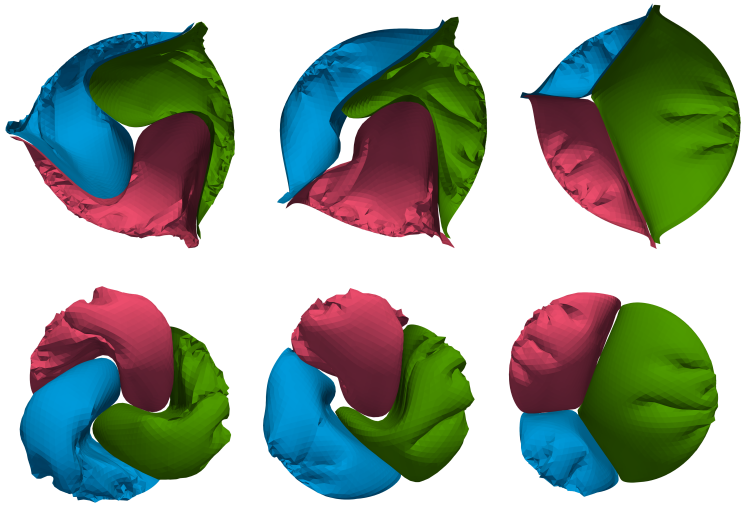

(a) (b) (c)

**Figure 8.** Results of three numerical experiments. The vertical columns show the results for virtual 'suturing' of (a) large equal cusps, (b) cusps of different inconsistent sizes, and (c) cusps with quasi-optimal intercommissural lengths. The horizontal rows show the dorsal and ventral views of the valve, the surrounding cylindrical aorta is not shown.

same time the dimensions of the cusps are such that they provide a tight closure of the entire valve (see Fig 8c). This means that the geometric relation formulated in Proposition 3.2 can be used to select the optimal geometry of the cusp templates.

All the above results show the presence of folds on the abdominal part of the template near the sutured border due to the nonlinear CSL-to-ASL suturing map. In surgical practice similar folds are observed as well.

## 5. Limitations

Despite the promising results, there are a number of shortcomings in this work. We did not investigate the suitability of the resulting 'sutured' states for carrying out further calculations on them. There may be difficulties associated with the collision processing which is inevitable for finding the diastolic configuration of the valve. We formulated the contact surfaces and carried out numerical experiments for an ideal cylindrical aortic root. A real geometry may produce new problems that were not identified in this article. Finally, in the proposed algorithm, the contact surface is imposed through the sequence of surfaces approaching to the required one. In the case of an arbitrary geometry, computation of a sign distance function for each surface may be an unacceptably computationally expensive operation.

## 6. Conclusions

We proposed the 'virtual suture' algorithm for initial placement of the aortic neo-cusps in which they are immersed in the lumen of the aortic root without neo-valve

prolapse, do not intersect with each other or with the surface of the aorta, the position of the cusp suture boundary satisfies the specified boundary conditions. The numerical experiments on the suturing of large cusps in the aortic region demonstrated the superiority of the proposed method over the method of virtual contact planes. The method is capable to place cusps of various sizes along ASLs with inconsistent sizes.

**Acknowledgment:** The author is grateful to Yuri Vassilevski and Victoria Salamatova for fruitful discussions and valuable comments.

## References

1. C. Alhan, Ozaki procedure. *Turkish Journal of Thoracic and Cardiovascular Surgery* **27** (2019), No. 4, 451.

2. C. W. Baird, S. P. Marathe, and P. J. Del Nido, Aortic valve neo-cuspidation using the Ozaki technique for acquired and congenital disease: where does this procedure currently stand? *Indian Journal of Thoracic and Cardiovascular Surgery* **36** (2020), No. 1, 113–122.

3. U. Benedetto, S. Sinha, A. Dimagli, L. Dixon, S. Stoica, L. Cocomello, C. Quarto, G. D. Angelini, U. Dandekar, and M. Caputo, Aortic valve neocuspidization with autologous pericardium in adult patients: Uk experience and meta-analytic comparison with other aortic valve substitutes. *European Journal of Cardio-Thoracic Surgery* **60** (2021), No. 1, 34–46.

4. R. Bridson, R. Fedkiw, and J. Anderson, Robust treatment of collisions, contact and friction for cloth animation. In: *Proc. of the 29th Annual Conference on Computer Graphics and Interactive Techniques*. 2002, pp. 594–603.

5. Y. Feng, Y. Cao, W. Wang, H. Zhang, L. Wei, B. Jia, and S. Wang, Computational modeling for surgical reconstruction of aortic valve by using autologous pericardium. *IEEE Access* **8** (2020), 97343–97352.

6. S. M. Hayama H., M. K. Hashimoto G., Y. H. Isekame Y., I. R. Ono T., and M. M. Hara H., Early detection of possible leaflet thrombosis after aortic valve neo-cuspidization surgery using autologous pericardium. In: *American Society of Echocardiography 29-th Annual Scientific Sessions, Vol. 31(6) J. Amer. Soc. Echocardiogr.* (2018).

7. A. C. Hindmarsh, R. Serban, C. J. Balos, D. J. Gardner, D. R. Reynolds, and C. S. Woodward, User documentation for kinsol v5.7.0 (sundials v5.7.0). Tech. Report, 2021.

8. Y. Iida, S. Akiyama, K. Shimura, S. Fujii, C. Hashimoto, S. Mizuuchi, Y. Arizuka, M. Nishioka, N. Shimura, S. Moriyama, et al., Comparison of aortic annulus dimensions after aortic valve neocuspidization with those of normal aortic valve using transthoracic echocardiography. *European Journal of Cardio-Thoracic Surgery* **54** (2018), No. 6, 1081–1084.

9. M. A. Jenkins and J. F. Traub, A three-stage algorithm for real polynomials using quadratic iteration. *SIAM Journal on Numerical Analysis* **7** (1970), No. 4, 545–566.

10. C. Kimberling, Encyclopedia of triangle centers (2022). http://faculty.evansville.edu/ck6/encyclopedia/ETC.html

11. T. Kunihara, D. Aicher, S. Rodionycheva, H.-V. Groesdonk, F. Langer, F. Sata, and H.-J. Schäfers, Preoperative aortic root geometry and postoperative cusp configuration primarily determine long-term outcome after valve-preserving aortic root repair. *Journal of Thoracic and Cardiovascular Surgery* **143** (2012), No. 6, 1389–1395.

12. J.-B. Le Polain De Waroux, A.-C. Pouleur, A. Robert, A. Pasquet, B. L. Gerber, P. Noirhomme, G. El Khoury, and J.-L. J. Vanoverschelde, Mechanisms of recurrent aortic regurgitation after aortic valve repair: predictive value of intraoperative transesophageal echocardiography. *JACC: Cardiovascular Imaging* **2** (2009), No. 8, 931–939.

13. K. Li and W. Sun, Simulated transcatheter aortic valve deformation: A parametric study on the impact of leaflet geometry on valve peak stress. *International Journal for Numerical Methods in Biomedical Engineering* **33** (2017), No. 3, e02814.

14. A. Liogky, P. Karavaikin, and V. Salamatova, Impact of material stiffness and anisotropy on coaptation characteristics for aortic valve cusps reconstructed from pericardium. *Mathematics* **9** (2021), No. 18, 2193.

15. S. Miyahara, A. Omura, T. Sakamoto, Y. Nomura, T. Inoue, H. Minami, K. Okada, and Y. Okita, Impact of postoperative cusp configuration on midterm durability after aortic root reimplantation. *Journal of Heart Valve Disease* **22** (2013), No. 4, 509–516.

16. S. Morganti, M. Conti, M. Aiello, A. Valentini, A. Mazzola, A. Reali, and F. Auricchio, Simulation of transcatheter aortic valve implantation through patient-specific finite element analysis: two clinical cases. *Journal of Biomechanics* **47** (2014), No. 11, 2547–2555.

17. W. H. Muller Jr, W. D. Warren, J. F. Dammann Jr, J. R. Beckwith, and J. E. Wood Jr, Surgical relief of aortic insufficiency by direct operation on the aortic valve. *Circulation* **21** (1960), No. 4, 587–597.

18. E. Oñate and F. G. Flores, Advances in the formulation of the rotation-free basic shell triangle. *Computer Methods in Applied Mechanics and Engineering* **194** (2005), No. 21-24, 2406–2443.

19. S. Ozaki, I. Kawase, H. Yamashita, S. Uchida, Y. Nozawa, T. Matsuyama, M. Takatoh, and S. Hagiwara, Aortic valve reconstruction using self-developed aortic valve plasty system in aortic valve disease. *Interactive Cardiovascular and Thoracic Surgery* **12** (2011), No. 4, 550–553.

20. S. Ozaki, I. Kawase, H. Yamashita, S. Uchida, M. Takatoh, S. Hagiwara, and N. Kiyohara, Aortic valve reconstruction using autologous pericardium for aortic stenosis. *Circulation Journal* **79** (2015), No. 7, 1504–1510.

21. Ozaki's procedure training video (2016) [cited 20.07.2022]. https://www.youtube.com/watch?v=Kww3ewKltfc

22. C. Ridley, B. Sohmer, P. Vallabhajosyula, and J. G. Augoustides, Aortic leaflet billowing as a risk factor for repair failure after aortic valve repair. *Journal of Cardiothoracic and Vascular Anesthesia* **31** (2017), No. 3, 1001–1006.

23. G. Rocatello, G. De Santis, S. De Bock, M. De Beule, P. Segers, and P. Mortier, Optimization of a transcatheter heart valve frame using patient-specific computer simulation. *Cardiovascular Engineering and Technology* **10** (2019), No. 3, 456–468.

24. H.-J. Schäfers, B. Bierbach, and D. Aicher, A new approach to the assessment of aortic cusp geometry. *Journal of Thoracic and Cardiovascular Surgery* **132** (2006), No. 2, 436–438.

25. P. Siondalski, L. Wilczynski, J. Rogowski, and M. Zembala, Human aortic bioprosthesis. *European Journal of Cardio-Thoracic Surgery* **34** (2008), No. 6, 1268–1268.

26. A. B. Tepole, H. Kabaria, K.-U. Bletzinger, and E. Kuhl, Isogeometric Kirchhoff–Love shell formulations for biological membranes. *Computer Methods in Applied Mechanics and Engineering* **293** (2015), 328–347.

27. Y. M. Thakeb, S. Sakr, E. El Sarawy, and A. M. Salem, Short-term competency of aortic valve repair in egyptian patients. *Journal of Cardiac Surgery* **35** (2020), No. 3, 598–602.

28. Y. Vassilevski, K. Terekhov, K. Nikitin, and I. Kapyrin, *Parallel Finite Volume Computation on General Meshes*. Springer, Cham, 2020.

29. Y. Vassilevski, A. Liogky, and V. Salamatova, Application of hyperelastic nodal force method to evaluation of aortic valve cusps coaptation: Thin shell vs. membrane formulations. *Mathematics* **9** (2021), No. 12, 1450.

30. Y. Yamamoto, K. Iino, Y. Shintani, H. Kato, K. Kimura, G. Watanabe, and H. Takemura, Comparison of aortic annulus dimension after aortic valve neocuspidization with valve replacement and normal valve. *Seminars in Thoracic and Cardiovascular Surgery* **29** (2017). No. 2, 143–149.

31. H. Zhu, Q. Yuan, X. Liu, and H. Cong, Fluid structure interaction analysis of transcatheter aortic valve implantation. *Chinese Journal of Tissue Engineering Research* (2019), 1599–1604.